THE JOURNAL OF PHYSICAL CHEMISTRY A
A JOURNAL OF THE AMERICAN CHEMICAL SOCIETY

pubs.acs.org/JPCA Article

# Chemical Reduction of $Ni^{II}$ Cyclam and Characterization of Isolated $Ni^{I}$ Cyclam with Cryogenic Vibrational Spectroscopy and Inert-Gas-Mediated High-Resolution Mass Spectrometry

*Published as part of The Journal of Physical Chemistry virtual special issue "Daniel Neumark Festschrift".*

Sean C. Edington, Evan H. Perez, David J. Charboneau, Fabian S. Menges, Nilay Hazari, and Mark A. Johnson*

Cite This: *J. Phys. Chem. A* 2021, 125, 6715–6721 Read Online

ACCESS | Metrics & More | Article Recommendations | Supporting Information

**ABSTRACT:** $Ni^{II}$ cyclam (cyclam = 1,4,8,11-tetraazacyclotetradecane) is an efficient catalyst for the selective reduction of $CO_2$ to CO. A crucial elementary step in the proposed catalytic cycle is the coordination of $CO_2$ to a $Ni^{I}$ cyclam intermediate. Isolation and spectroscopic characterization of this labile $Ni^{I}$ species without solvent has proven to be challenging, however, and only partial IR spectra have previously been reported using multiple photon fragmentation of ions generated by gas-phase electron transfer to the $Ni^{II}$ cyclam dication at 300 K. Here, we report a chemical reduction method that efficiently prepares $Ni^{I}$ cyclam in solution. This enables the $Ni^{I}$ complex to be transferred into a cryogenic photofragmentation mass spectrometer using inert-gas-mediated electrospray ionization. The vibrational spectra of the 30 K ion using both $H_2$ and $N_2$ messenger tagging over the range 800−4000 $cm^{-1}$ were then measured. The resulting spectra were analyzed with the aid of electronic structure calculations, which show strong method dependence in predicted band positions and small molecule activation. The conformational changes of the cyclam ligand induced by binding of the open shell $Ni^{I}$ cation were compared with those caused by the spherical, closed-shell $Li^{I}$ cation, which has a similar ionic radius. We also report the vibrational spectrum of a $Ni^{I}$ cyclam complex with a strongly bound $O_2$ ligand. The cyclam ligand supporting this species exhibits a large conformational change compared to the complexes with weakly bound $N_2$ and $H_2$, which is likely due to significant charge transfer from Ni to the coordinated $O_2$.

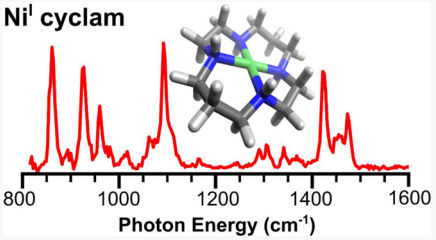


## I. INTRODUCTION

A major challenge in chemistry is to determine the structure and reactivity of intermediates formed in catalysis.[1−7] These species often have short lifetimes and are too unstable to analyze using traditional techniques, such as X-ray diffraction or NMR spectroscopy. For example, the coordination and activation of $CO_2$ by reactive transition metal complexes is proposed to be a crucial elementary step in the catalytic conversion of $CO_2$ to a range of more valuable chemicals including CO and methanol.[8−13] The present literature, however, rarely explores the binding of $CO_2$ to the highly reactive and unstable complexes that are purported as intermediates in catalysis but rather typically focuses on more stable model complexes.[14−17] Here, we investigate Ni complexes supported by the planar macrocyclic cyclam (cyclam = 1,4,8,11- tetraazacyclotetradecane, hereafter denoted "L1") ligand (Figure 1). Complexes of the this type are efficient and selective electrocatalysts for the reduction of $CO_2$ to CO[18] with the $Ni^{I}$-L1 intermediate hypothesized to play a key role in the high selectivity,[19−21] but experimental information about the structure of $Ni^{I}$-L1 is limited.[22]

A recently developed method for studying the activation of small molecules in compounds such as $Ni^{I}$-L1 involves isolating the singly charged molecular cations in the gas phase with open coordination sites on the metal center and then attaching substrates in a temperature-controlled ion trap.[23−28] This approach follows earlier methods for the study of intermediates that employed an infrared-ultraviolet double-resonance scheme for acquiring the vibrational spectra of cold

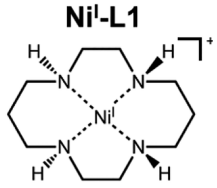


**Figure 1.** Schematic structure of the *trans-III* isomer of $Ni^{I}$-L1.

**Received:** June 7, 2021
**Revised:** July 14, 2021
**Published:** July 29, 2021







https://doi.org/10.1021/acs.jpca.1c05016
*J. Phys. Chem. A* 2021, 125, 6715–6721

ions.[29] Although a related gas-phase method was successful for studying $CO_2$ binding to a $Ni^I$ complex with a specifically designed, noncatalytic ligand system,[30,31] it has been difficult to efficiently prepare the key $Ni^I$-L1 complex in a manner compatible with cryogenic ion spectroscopy. The only reported characterization of the $Ni^I$-L1 cation in isolation involved a scheme that employed exothermic gas-phase electron transfer to the stable $Ni^{II}$-L1 complex[32−35] followed by buffer gas cooling to 300 K and reported the vibrational spectrum only in the fingerprint region (600−1600 $cm^{-1}$).

Here, we describe an alternative method involving chemical reduction of the stable $Ni^{II}$-L1 compound with decamethylcobaltocene ($((C_5(CH_3)_5)_2Co^{II}$), hereafter denoted $(Cp^*)_2Co$) to generate $Ni^I$-L1 cations in solution. These ions are extracted into the gas phase using electrospray ionization (ESI) and characterized at low temperature via vibrational spectroscopy. Spectra are recorded using the messenger tagging approach, where weakly bound $H_2$ and $N_2$ complexes prepared in a cryogenic (30 K) radiofrequency ion trap undergo infrared photodissociation (IRPD). The resulting band patterns in the 800−4000 $cm^{-1}$ range are compared with predictions from a variety of computational methods. Surprisingly, the computational predictions of small-molecule activation by $Ni^I$-L1 show strong method dependence, which indicates there are challenges associated with calculating the structure of these complexes. We compared the experimental structure of $Ni^I$-L1 with $Li^I$-L1, which contains a closed-shell metal center. This enabled us to determine the impact of the Ni d electrons on the binding of the L1 ligand and determine that cyclam binding is primarily governed by electrostatic factors. Finally, using $O_2$ as a substrate, we demonstrate that it is possible to bind a more reactive molecule than $N_2$ or $H_2$ to the $Ni^I$ center by carrying out a three-body attachment of $O_2$ in an ion guide. The resulting complex was characterized using cryogenic vibrational spectroscopy.

## II. EXPERIMENTAL METHODS

**IIA. Oxidation State Control.** The stable $Ni^{II}$-L1 $PF_6$ salt was reduced with a slight excess of $(Cp^*)_2Co$ in dry and deoxygenated acetonitrile to generate $Ni^I$-L1. The reduction was performed in a glovebox, and the products were transferred to a gastight syringe (Hamilton Company) for transport and injection into the ion source. This method generates a solution containing the $Ni^I$-L1 cation that is stable for several hours under the oxygen- and water-free conditions maintained by the syringe. Samples were analyzed with the Yale hybrid photofragmentation mass spectrometer, which has been described previously.[26] In short, the instrument combines a commercial ThermoFisher Orbitrap Velos Pro mass spectrometer (hereafter denoted "Orbitrap") with a custom-built, double-focusing tandem time-of-flight photofragmentation mass spectrometer. Electrospray ionization of the $Ni^I$-L1 solution described above carried out with the Orbitrap's ion source using $N_2$ sheath gas yields the mass spectrum (hereafter denoted "MS") in Figure 2b. This is compared with the MS from the $Ni^{II}$-L1 sample solution prior to reduction with $(Cp^*)_2Co$ in panel Figure 2a. These results highlight the utility of the Orbitrap's high resolution capability by confirming successful synthesis of the labile $Ni^I$ intermediate before transfer to the photofragmentation spectrometer. Specifically, this capability allowed unambiguous identification of a minor deprotonated $Ni^{II}$-L1 contaminant, which is formed during generation of $Ni^I$-L1 (Figure 2b).

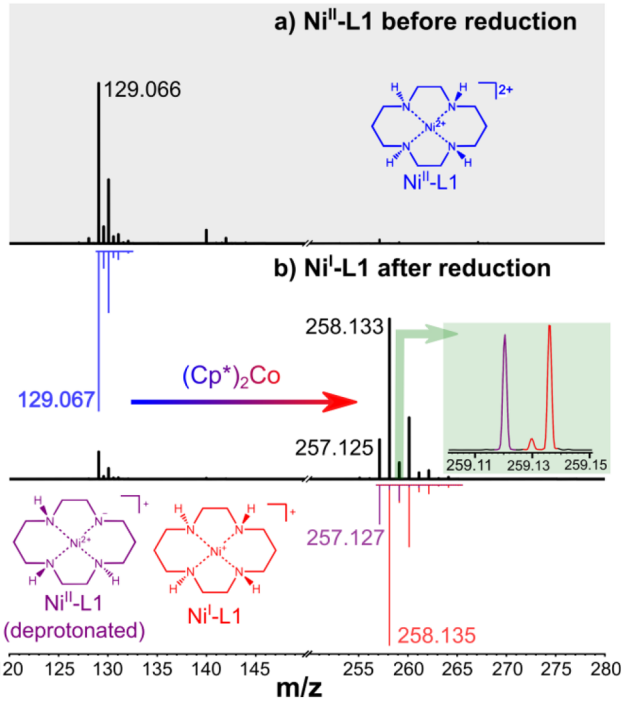


**Figure 2.** High resolution mass spectrometric preparation and isolation of the $Ni^I$-L1 cation. a) Mass spectrum of unreduced $Ni^{II}$-L1 and b) $Ni^I$-L1 generated by reduction with $(Cp^*)_2Co$ in solution. Isotopic pattern simulations are color-coded to the inset chemical structures and inverted underneath the experimental data. The isotopic pattern of the reduced sample b) is in excellent agreement with the expected combined mass spectrum for $Ni^I$-L1 and a lower abundance of the deprotonated $Ni^{II}$-L1 complex. The $Ni^{II}$ species is expected to contribute less than 5% to the peak around $m/z$ 258 that was isolated for spectroscopic characterization. The green-shaded inset in panel b) expands the $m/z$ axis scale to demonstrate the Orbitrap's capability to resolve the features of $Ni^I$-L1 and deprotonated $Ni^{II}$-L1, which are separated by less than 0.05 $m/z$.

## III. RESULTS AND DISCUSSION

**IIIA. Mass Isolation of $Ni^I$ Complexes and Spectroscopic Verification of Product Oxidation State.** To verify that the present solution-phase preparation yields the same structures as the gas-phase approaches employed in our previous work,[30,31] we applied the synthesis described above to another $Ni^I$ complex whose IRPD spectrum we earlier acquired following gas-phase synthesis: $Ni^I$-L-$N_4Me_2$ (L-$N_4Me_2$ = *N,N′*-dimethyl-2,11-diaza[3,3](2,6)pyridinophane, hereafter denoted "L2"). Those experiments generated the coordinatively unsaturated $Ni^I$-L2 center by collisional dissociation of a stable $Ni^I$ precursor ion in the gas phase.[30,31] The solution chemistry applied to the generation of $Ni^I$-L1 indeed provides an alternative route to this $Ni^I$-L2 species: comparison of $Ni^I$-L2 infrared spectra taken as part of the present study and those reported previously (Figure S1) confirms that both solution- and gas-phase methods produce the same forms of the cation. We note that isolating the desired $Ni^I$-L2 ($m/z$ = 326.104) cation from this reaction mixture with ESI is challenging because the spray yields an intense peak at $m/z$ = 329 due to the oxidized reducing agent, $[(Cp^*)_2Co^{III}]^+$ (329.168 $m/z$), which saturates the ion trap required for the spectroscopy experiments, thus suppressing the yield of the target $Ni^I$-L2 cation. This problem was overcome using the Orbitrap's mass isolation function to select $m/z$ = 326 prior to injection into


https://doi.org/10.1021/acs.jpca.1c05016
J. Phys. Chem. A 2021, 125, 6715−6721

the photofragmentation mass spectrometer, as illustrated by the mass spectra before and after isolation in Figure S2.

**IIIB. Vibrational Spectrum of $Ni^I$-L1 at 30 K Using $H_2$ Tagging.** The ability to generate robust yields of Ni-L1 in the critical $Ni^I$ oxidation state enables the acquisition of its vibrational spectrum in a linear action regime using cryogenic IR photodissociation of complexes with weakly bound "mass tags". This represents a significant advance because the previous spectroscopic study of this system[32] was limited to the 800−1600 $cm^{-1}$ range and was obtained using 300 K infrared multiphoton dissociation (IRMPD) of the bare ion. Here, we report the spectrum of the $Ni^I$-L1-2$H_2$ cluster ion, where the $H_2$ tags are expected to bind to the $Ni^I$ metal center, over the range 800−4100 $cm^{-1}$ (Figures 3a and 4b). This is

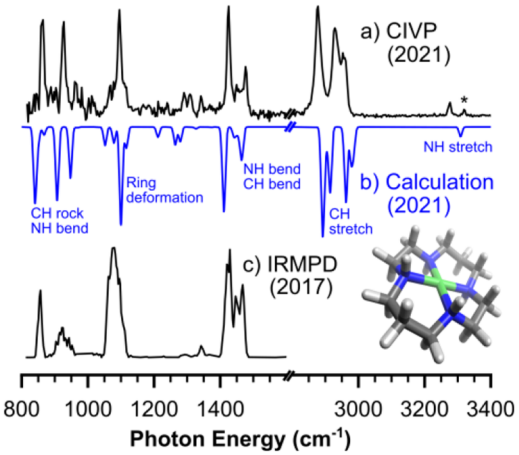


**Figure 3.** Comparison between the vibrational spectra of the $Ni^I$-L1 cation obtained by a) vibrational predissociation of the $Ni^I$-L1-2$H_2$ cluster at 30 K and c) 300 K IRMPD of the bare ion reproduced from an earlier report.[32] The calculated spectrum of the *trans-III* isomer of the bare $Ni^I$-L1 cation (M06-2X/SDD, scaled by 0.95) is displayed in b) along with qualitative descriptions of the modes involved in the various fundamentals. The corresponding minimum-energy structure is shown as an inset. The asterisk marks a feature which we do not assign. The observed tag-dependent multiplet structure in the region expected for the NH stretching modes (see Figure S4) is not predicted at the harmonic level.

compared with the predicted harmonic spectrum (Figure 3b) and previously acquired IRMPD spectrum (Figure 3c) of bare $Ni^I$-L1, whose minimum energy structure is displayed in the Figure 3 inset. The doubly tagged (2$H_2$) complex was chosen to avoid mass overlap between the $^{60}Ni^I$-L1 isotopologue of the bare cation and $^{58}Ni^I$-L1-$H_2$. The $H_2$ molecules were observed to attach at approximately 40 K, which is typical for operation in the tagging regime where the spectra of the $H_2$ complexes are observed to be very close to those of the isolated, cold parent ions.[36] Further evidence of the weak interaction between $Ni^I$-L1 and $H_2$ is the fact that the $H_2$ stretching fundamental is weak and observed at 4137 $cm^{-1}$ (Figure 4b, blue line), very close to the value (4161 $cm^{-1}$, gray line in Figure 4) in isolated $H_2$.[37] The $H_2$ molecule is predicted, at the M06-2X/SDD level of theory,[38−41] to attach by primarily electrostatic interaction with the metal center in an "end-on" arrangement as indicated in the structure displayed in Figure S3. Activation of the IR-forbidden diatomic stretching transitions is attributable to polarization of, and charge transfer to, the diatomic tag by the molecular ion. This behavior and the expected relationship between transition strength and red shift (transition strength and red shift increase together) has been treated in previous work and agrees with the trends observed here.[42−47] Red shifts of the $H_2$ stretching transitions observed in this work are summarized in Figures S5 and S6.

The spectrum of the $Ni^I$-L1-2$H_2$ ion at 30 K in Figure 3a generally displays features in the same locations as those observed with IRMPD of room temperature ions (Figure 3c). As expected, the relative intensities are somewhat different—and the features better resolved—in the linear spectrum of the cold ion. However, this technique also introduces the possibility that the tag molecules perturb the intrinsic structure and vibrational band pattern of the isolated $Ni^I$-L1 cation. To address this issue, we noted that $N_2$ attachment to form the $Ni^I$-L1-$N_2$ cluster ion occurred at a similarly low temperature, suggesting that $N_2$ is also very weakly bound[46,47] to the molecular cation. The observed IRPD spectra of the $H_2$- and $N_2$-tagged ions are compared in Figure 4. These spectra are essentially identical with the exception of tag-dependent multiplet structure (labeled *) in the NH stretching region (Figure S4), which is evident in the features near 3300 $cm^{-1}$ in Figure 4a and 4b. This overall similarity, combined with the fact that the $N_2$ stretch is extremely weak and occurs at 2328 $cm^{-1}$, very close to the 2330 $cm^{-1}$ value of the N−N stretching vibration[48] in free $N_2$(red vertical line in Figure 4), lends strong support to the conclusion that the tag molecules do not significantly affect the band pattern, and hence structure, of the isolated ion.

The greatest advantage of the tagging method for acquiring vibrational spectra is that the band patterns can be directly compared with (scaled) harmonic predictions of the absorption spectra predicted for candidate minimum energy structures. In the case of $Ni^I$-L1, there are two dominant isomeric forms[20] that differ according to the orientation of the NH groups (the so-called *trans-I* and *trans-III* isomers, shown in Figure S7). The spectrum calculated (M06-2X/SDD) for the *trans-III* isomer, which is predicted to lie ∼3.5 kJ/mol lower in energy than the *trans-I* form, is presented in Figure 3b and is in excellent agreement with the observed pattern. A comparison of the observed spectrum with those calculated for the *trans-I* and *trans-III* isomers is presented in Figure S7. The agreement in the lower energy region near 1000 $cm^{-1}$ for the *trans-III* isomer is particularly compelling. Specifically, the strong narrow peak corresponding to the ring deformation in the *trans-I* spectrum is predicted to degrade into a plethora of bands in the *trans-III* spectrum. We note that the *trans-III* form was identified as the isomer generated in the gas phase in the earlier report.[32] Finally, it is valuable to acknowledge how strongly the calculated spectra depend on the choice of DFT functionals and basis sets. Figure S8 illustrates the surprisingly large variations in the harmonic spectra of $Ni^I$-L1-$N_2$ calculated using 28 different combinations of functionals and basis sets. Remarkably, the harmonic predictions for $N_2$ stretching frequencies span a range of ∼1200 $cm^{-1}$. This work does not seek to identify the cause of this variation but rather to report the linear experimental spectrum and thus provide an experimental benchmark to guide future theoretical efforts. It is useful to note, however, that the large variation only occurs in the frequency of the $N_2$ stretch; the general pattern of bands from scaffold are largely consistent across the methods surveyed.


https://doi.org/10.1021/acs.jpca.1c05016
J. Phys. Chem. A 2021, 125, 6715−6721

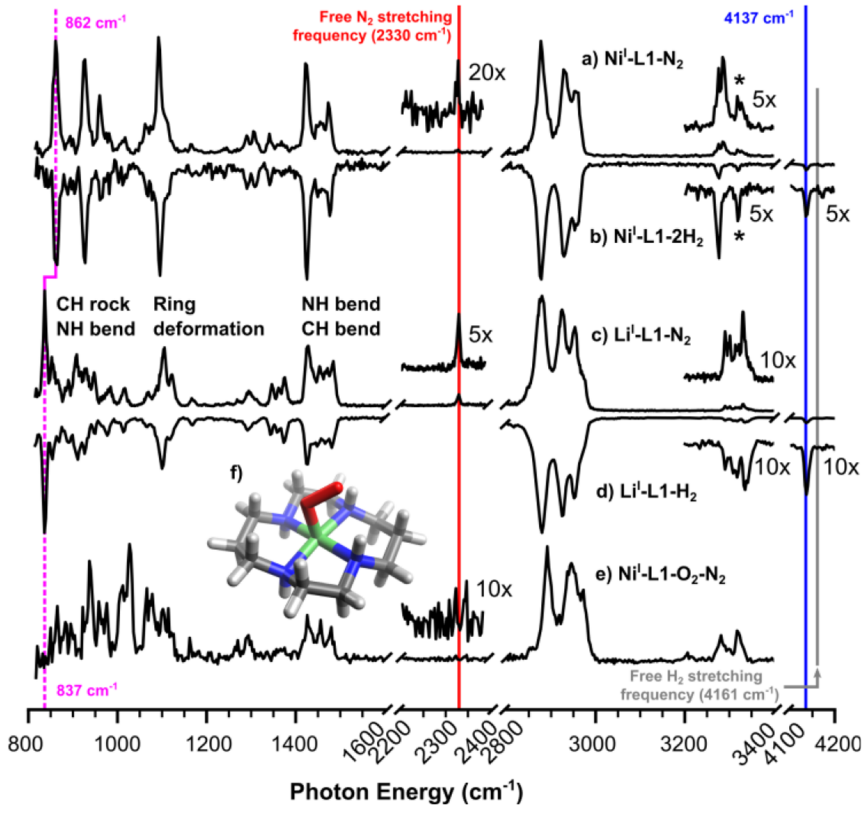


**Figure 4.** CIVP spectra of the cations a) $Ni^{I}$-L1-$N_2$, b) $Ni^{I}$-L1-$2H_2$, c) $Li^{I}$-L1-$N_2$, d) $Li^{I}$-L1-$H_2$, and e) $Ni^{I}$-L1-$O_2$-$N_2$. The structure of $Ni^{I}$-L1-$O_2$ predicted at the M06-2X/SDD level of theory is included in f).

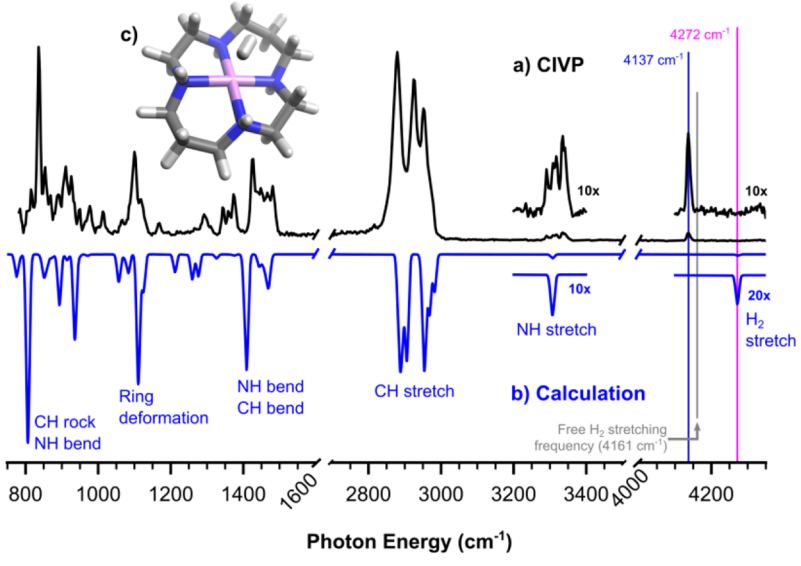


**Figure 5.** Comparison of the a) experimental and b) predicted (M06-2X/SDD, scaled by 0.95) vibrational spectra of $Li^{I}$-L1-$H_2$. The predicted minimum energy structure is shown in c).

**IIIC. Investigation of Metal-Ion-Dependent Scaffold Deformation.** The large variation in theoretical predictions for the interactions between $Ni^{I}$-L1 and $N_2$ highlights the challenges for widely accessible electronic structure theory to accurately predict the behavior of the open shell (nominally $d^9$) $Ni^{I}$ ion. To empirically explore the extent to which the response of the cyclam ligand is primarily electrostatic in character, we recorded the vibrational spectra of the $Li^{I}$ analogues $Li^{I}$-L1-$H_2$ and $Li^{I}$-L1-$N_2$ (Figure 5a and Figure 4c and 4d), which are compared to the $Ni^{I}$-L1-$2H_2$ and $Ni^{I}$-L1-$N_2$ spectra in Figure 4a–4d, respectively. The bands associated with the complexes tagged by either $H_2$ and $N_2$ are once again essentially identical: the positions of all bands remain within the ~3 $cm^{-1}$ bandwidth of our laser on moving from the $H_2$ to $N_2$ tags. A survey of predicted $Li^{I}$-L1-$N_2$ spectra (Figure S9) using the same methods applied to the $Ni^{I}$-L1-$N_2$ complex (Figure S8) shows that the calculated $N_2$ stretching transitions


https://doi.org/10.1021/acs.jpca.1c05016
J. Phys. Chem. A 2021, 125, 6715–6721

are much more consistent in intensity, but still vary over a large ~700 $cm^{-1}$ range of frequencies.

The experimental spectrum for $Li^{I}$-L1-$H_2$ is compared with the harmonic prediction in Figure 5 to illustrate the performance of the M06-2X/SDD level of theory. The predicted bands in the CH region are very accurate, and the CH/NH bending and ring deformation features in the fingerprint region are also satisfactory. Weaker bands in the CH rock/NH bend region involving collective motions are in worse agreement, however, as are the NH stretches near 3300 $cm^{-1}$. Thus, the poor agreement with the NH stretching bands mentioned above cannot be solely attributed to complications arising from the open shell $d^9$ configuration of the $Ni^{I}$ cation.

The most important result from this study is that we have established a robust method to generate catalytically relevant $Ni^{I}$-L1. In principle, this enables the investigation of the reactivity of $Ni^{I}$-L1 with small molecules, which has previously been challenging. As a demonstration of this capability, we attached $O_2$ to $Ni^{I}$-L1 by introducing $O_2$ into an ion guide that transfers the cation to the cryogenic ion trap at ambient temperature. The fact that $O_2$ binds at such high temperature confirms that the $O_2$ is very strongly bound to the metal center. Since the resulting $Ni^{I}$-L1-$O_2$ complex is too tightly bound to allow the collection of photofragmentation spectra below ~2500 $cm^{-1}$ in a linear regime, the $O_2$ complex was tagged with $N_2$ in the cryogenic ion trap at 40 K. The vibrational spectrum of $Ni^{I}$-L1-$O_2$-$N_2$ ion is displayed in Figure 4e. As evidenced by the dramatic changes in the fingerprint-region band pattern relative to those of the isolated ion Figure 4a–d, attachment of $O_2$ indeed induces substantial rearrangement of the ligand. The calculated structure of the $O_2$ complex is displayed in Figure 4f and features substantial charge transfer to $O_2$. These large changes in the ligand bands are easily rationalized by considering the substantial charge redistribution between the $Ni^{I}$-L1 complex and the $O_2$ substrate. Calculations at the same level of theory applied to the bare cation indicate about 0.5 $e^-$ is transferred from Ni to the $O_2$ moiety. The band associated with the $O_2$ stretch, which is predicted to be weak and fall in the congested fingerprint region at around 1100 $cm^{-1}$, was not readily identified by inspection.[49]

Unfortunately, our attempts to isolate $CO_2$ bound to $Ni^{I}$-L1 using this approach were not successful, indicating that this interaction is weak compared to the behavior of the nominally similar $Ni^{I}$-L2 system that readily attaches $CO_2$ at elevated temperature.[30] This difference raises the issue of how the local coordination environment around the $Ni^{I}$ ion drives chemical interactions with small molecules. This aspect of $Ni^{I}$ coordination chemistry can be addressed by introducing a solvent molecule to one of the two open sites on the metal center in the planar cyclam scaffold before condensing $CO_2$ onto the remaining open site. Modifications to the instrument are currently underway to explore how substrate activation responds to such manipulations of the coordination environment around the $Ni^{I}$ metal center.

## IV. CONCLUSION

We have demonstrated an efficient method to isolate $Ni^{I}$-cyclam with the metal ion in the labile $Ni^{I}$ oxidation state. This approach enables the characterization of $Ni^{I}$-cyclam with high-resolution mass spectrometry and cryogenic vibrational spectroscopy. The $Ni^{I}$ cyclam cation was generated by chemical reduction of the stable $Ni^{II}$ cyclam dication in solution and then isolated by extraction into a photofragmentation mass spectrometer. Isolated $Ni^{I}$-cyclam displayed relatively inert chemical behavior toward $N_2$ and $H_2$ and appears similar in terms of both structure and chemical activity to $Li^{I}$-cyclam, which was chosen to preserve the charge and size of the central ion, while eliminating contributions from d-orbitals. The isolated $Ni^{I}$-cyclam cation binds $O_2$ very strongly, and its vibrational spectrum reveals substantial distortion of the cyclam ligand, consistent with partial charge transfer to the $O_2$ substrate. The methods reported here provide a useful protocol for investigating the intrinsic interactions of this system with catalytically relevant substrates, and further work is ongoing to explore the role of solvent coordination in the activation of small molecule substrates, such as $CO_2$.

## ■ ASSOCIATED CONTENT

### Supporting Information

The Supporting Information is available free of charge at https://pubs.acs.org/doi/10.1021/acs.jpca.1c05016.

Experimental methods; computational methods; summary of molecular names, formulas, and masses; comparison of present $Ni^{I}$-L2 CIVP spectra and predicted harmonic spectra with previously published results; demonstration of hybrid instrument mass isolation capability; minimum energy structure of $Ni^{I}$-L1-$H_2$; demonstration of tag-dependent multiplet structure in $Ni^{I}$-L1 NH stretching region; comparison of $Ni^{I}$-L1 CIVP spectra with predicted harmonic spectra of *trans-III* and *trans-I* isomers; comparison of $Ni^{I}$-L1 and $Li^{I}$-L1 CIVP spectra with harmonic spectra predicted for same using different functional/basis set combinations; summary of $H_2$ stretching fundamental red shifts in $H_2$-tagged complexes. (PDF)

## ■ AUTHOR INFORMATION


### Corresponding Author

**Mark A. Johnson** − *Sterling Chemistry Laboratory, Chemistry Department, Yale University, New Haven, Connecticut 06520, United States;* orcid.org/0000-0002-1492-6993; Email: mark.johnson@yale.edu

### Authors

**Sean C. Edington** − *Sterling Chemistry Laboratory, Chemistry Department, Yale University, New Haven, Connecticut 06520, United States;* orcid.org/0000-0002-5894-8801

**Evan H. Perez** − *Sterling Chemistry Laboratory, Chemistry Department, Yale University, New Haven, Connecticut 06520, United States*

**David J. Charboneau** − *Sterling Chemistry Laboratory, Chemistry Department, Yale University, New Haven, Connecticut 06520, United States*

**Fabian S. Menges** − *Sterling Chemistry Laboratory, Chemistry Department, Yale University, New Haven, Connecticut 06520, United States;* orcid.org/0000-0002-5859-9197

**Nilay Hazari** − *Sterling Chemistry Laboratory, Chemistry Department, Yale University, New Haven, Connecticut 06520, United States;* orcid.org/0000-0001-8337-198X

Complete contact information is available at: https://pubs.acs.org/10.1021/acs.jpca.1c05016


### Notes

The authors declare no competing financial interest.



https://doi.org/10.1021/acs.jpca.1c05016
J. Phys. Chem. A 2021, 125, 6715−6721

## ■ ACKNOWLEDGMENTS

M.A.J. thanks the Air Force Office of Scientific Research (AFOSR) under grant FA9550-17-1-0267 and acknowledges that the study was carried out using an instrument developed under (DURIP) FA9550-18-1-0213. N.H. acknowledges support from the NIHGMS under Award Number R01GM120162. We thank Prof. Hans-Jörg Krueger (Univ. Kaiserslautern) for providing a sample of the L2 ligand. LCMS based chemical analyses critical to this study regarding the purity of the ligands was obtained using a high-resolution mass spectrometer provided under NSF MRI grant CHE-1828190.

## ■ REFERENCES

(1) Neri, G.; Walsh, J. J.; Teobaldi, G.; Donaldson, P. M.; Cowan, A. J. Detection of catalytic intermediates at an electrode surface during carbon dioxide reduction by an earth-abundant catalyst. *Nat. Catal.* **2018**, *1* (12), 952−959.

(2) Hemberger, P.; Custodis, V. B. F.; Bodi, A.; Gerber, T.; van Bokhoven, J. A. Understanding the mechanism of catalytic fast pyrolysis by unveiling reactive intermediates in heterogeneous catalysis. *Nat. Commun.* **2017**, *8* (1), 15946.

(3) Goswami, M.; Chirila, A.; Rebreyend, C.; de Bruin, B. EPR Spectroscopy as a Tool in Homogeneous Catalysis Research. *Top. Catal.* **2015**, *58* (12), 719−750.

(4) Tsang, A. S. K.; Sanhueza, I. A.; Schoenebeck, F. Combining Experimental and Computational Studies to Understand and Predict Reactivities of Relevance to Homogeneous Catalysis. *Chem. - Eur. J.* **2014**, *20* (50), 16432−16441.

(5) Vikse, K. L.; Ahmadi, Z.; Scott McIndoe, J. The application of electrospray ionization mass spectrometry to homogeneous catalysis. *Coord. Chem. Rev.* **2014**, *279*, 96−114.

(6) Gustafson, K. P. J.; Guđmundsson, A.; Bajnóczi, É. G.; Yuan, N.; Zou, X.; Persson, I.; Bäckvall, J.-E. In Situ Structural Determination of a Homogeneous Ruthenium Racemization Catalyst and Its Activated Intermediates Using X-Ray Absorption Spectroscopy. *Chem. - Eur. J.* **2020**, *26* (15), 3411−3419.

(7) MacMillan, S. N.; Lancaster, K. M. X-ray Spectroscopic Interrogation of Transition-Metal-Mediated Homogeneous Catalysis: Primer and Case Studies. *ACS Catal.* **2017**, *7* (3), 1776−1791.

(8) Burkart, M. D.; Hazari, N.; Tway, C. L.; Zeitler, E. L. Opportunities and Challenges for Catalysis in Carbon Dioxide Utilization. *ACS Catal.* **2019**, *9* (9), 7937−7956.

(9) Ra, E. C.; Kim, K. Y.; Kim, E. H.; Lee, H.; An, K.; Lee, J. S. Recycling Carbon Dioxide through Catalytic Hydrogenation: Recent Key Developments and Perspectives. *ACS Catal.* **2020**, *10* (19), 11318−11345.

(10) Artz, J.; Müller, T. E.; Thenert, K.; Kleinekorte, J.; Meys, R.; Sternberg, A.; Bardow, A.; Leitner, W. Sustainable Conversion of Carbon Dioxide: An Integrated Review of Catalysis and Life Cycle Assessment. *Chem. Rev.* **2018**, *118* (2), 434−504.

(11) Álvarez, A.; Bansode, A.; Urakawa, A.; Bavykina, A. V.; Wezendonk, T. A.; Makkee, M.; Gascon, J.; Kapteijn, F. Challenges in the Greener Production of Formates/Formic Acid, Methanol, and DME by Heterogeneously Catalyzed $CO_2$ Hydrogenation Processes. *Chem. Rev.* **2017**, *117* (14), 9804−9838.

(12) Sordakis, K.; Tang, C.; Vogt, L. K.; Junge, H.; Dyson, P. J.; Beller, M.; Laurenczy, G. Homogeneous Catalysis for Sustainable Hydrogen Storage in Formic Acid and Alcohols. *Chem. Rev. (Washington, DC, U. S.)* **2018**, *118* (2), 372−433.

(13) Zimmermann, P.; Kilpatrick, A. F. R.; Ar, D.; Demeshko, S.; Cula, B.; Limberg, C. Electron transfer within beta-diketiminato nickel bromide and cobaltocene redox couples activating $CO_2$. *Chem. Commun.* **2021**, *57* (7), 875−878.

(14) Francke, R.; Schille, B.; Roemelt, M. Homogeneously Catalyzed Electroreduction of Carbon Dioxide—Methods, Mechanisms, and Catalysts. *Chem. Rev.* **2018**, *118* (9), 4631−4701.

(15) Schwarz, H. Metal-Mediated Activation of Carbon Dioxide in the Gas Phase: Mechanistic Insight Derived from a Combined Experimental/Computational Approach. *Coord. Chem. Rev.* **2017**, *334*, 112−123.

(16) Yang, H. B.; Hung, S. F.; Liu, S.; Yuan, K. D.; Miao, S.; Zhang, L. P.; Huang, X.; Wang, H. Y.; Cai, W. Z.; Chen, R.; et al. Atomically dispersed Ni(I) as the active site for electrochemical $CO_2$ reduction. *Nat. Energy* **2018**, *3* (2), 140−147.

(17) Dodson, L. G.; Thompson, M. C.; Weber, J. M. Characterization of Intermediate Oxidation States in $CO_2$ Activation. *Annu. Rev. Phys. Chem.* **2018**, *69*, 231−252.

(18) Beley, M.; Collin, J.-P.; Ruppert, R.; Sauvage, J.-P. Nickel(II)-cyclam: an extremely selective electrocatalyst for reduction of $CO_2$ in water. *J. Chem. Soc., Chem. Commun.* **1984**, No. 19, 1315−1316.

(19) Froehlich, J. D.; Kubiak, C. P. The Homogeneous Reduction of $CO_2$ by $[Ni(cyclam)]^+$: Increased Catalytic Rates with the Addition of a CO Scavenger. *J. Am. Chem. Soc.* **2015**, *137* (10), 3565−3573.

(20) Froehlich, J. D.; Kubiak, C. P. Homogeneous $CO_2$ Reduction by Ni(cyclam) at a Glassy Carbon Electrode. *Inorg. Chem.* **2012**, *51* (7), 3932−3934.

(21) Song, J.; Klein, E. L.; Neese, F.; Ye, S. The Mechanism of Homogeneous $CO_2$ Reduction by Ni(cyclam): Product Selectivity, Concerted Proton-Electron Transfer and C-O Bond Cleavage. *Inorg. Chem.* **2014**, *53* (14), 7500−7507.

(22) Behnke, S. L.; Manesis, A. C.; Shafaat, H. S. Spectroelectrochemical investigations of nickel cyclam indicate different reaction mechanisms for electrocatalytic $CO_2$ and $H^+$ reduction. *Dalton Trans.* **2018**, *47* (42), 15206−15216.

(23) Wolk, A. B.; Leavitt, C. M.; Garand, E.; Johnson, M. A. Cryogenic Ion Chemistry and Spectroscopy. *Acc. Chem. Res.* **2014**, *47* (1), 202−210.

(24) Roithová, J.; Gray, A.; Andris, E.; Jašík, J.; Gerlich, D. Helium Tagging Infrared Photodissociation Spectroscopy of Reactive Ions. *Acc. Chem. Res.* **2016**, *49* (2), 223−230.

(25) Roithová, J. Characterization of reaction intermediates by ion spectroscopy. *Chem. Soc. Rev.* **2012**, *41* (2), 547−559.

(26) Menges, F. S.; Perez, E. H.; Edington, S. C.; Duong, C. H.; Yang, N.; Johnson, M. A. Integration of High-Resolution Mass Spectrometry with Cryogenic Ion Vibrational Spectroscopy. *J. Am. Soc. Mass Spectrom.* **2019**, *30* (9), 1551−1557.

(27) Schwarz, H.; Asmis, K. R. Identification of Active Sites and Structural Characterization of Reactive Ionic Intermediates by Cryogenic Ion Trap Vibrational Spectroscopy. *Chem. - Eur. J.* **2019**, *25* (9), 2112−2126.

(28) Kamrath, M. Z.; Rizzo, T. R. Combining Ion Mobility and Cryogenic Spectroscopy for Structural and Analytical Studies of Biomolecular Ions. *Acc. Chem. Res.* **2018**, *51* (6), 1487−1495.

(29) Fedorov, A.; Couzijn, E. P. A.; Nagornova, N. S.; Boyarkin, O. V.; Rizzo, T. R.; Chen, P. Structure and Bonding of Isoleptic Coinage Metal (Cu, Ag, Au) Dimethylaminonitrenes in the Gas Phase. *J. Am. Chem. Soc.* **2010**, *132* (39), 13789−13798.

(30) Menges, F. S.; Craig, S. M.; Totsch, N.; Bloomfield, A.; Ghosh, S.; Kruger, H. J.; Johnson, M. A. Capture of $CO_2$ by a Cationic Nickel(I) Complex in the Gas Phase and Characterization of the Bound, Activated $CO_2$ Molecule by Cryogenic Ion Vibrational Predissociation Spectroscopy. *Angew. Chem., Int. Ed.* **2016**, *55* (4), 1282−1285.

(31) Craig, S. M.; Menges, F. S.; Johnson, M. A. Application of Gas Phase Cryogenic Vibrational Spectroscopy to Characterize the $CO_2$, CO, $N_2$ and $N_2O$ Interactions With the Open Coordination Site on a Ni(I) Macrocycle Using Dual Cryogenic Ion Traps. *J. Mol. Spectrosc.* **2017**, *332*, 117−123.

(32) Munshi, M. U.; Craig, S. M.; Berden, G.; Martens, J.; DeBlase, A. F.; Forman, D. J.; McLuckey, S. A.; Oomens, J.; Johnson, M. A. Preparation of Labile $Ni^+$(cyclam) Cations in the Gas Phase Using Electron Transfer Reduction through Ion-ion Recombination in an Ion Trap and Structural Characterization with Vibrational Spectroscopy. *J. Phys. Chem. Lett.* **2017**, *8*, 5047−5052.



https://doi.org/10.1021/acs.jpca.1c05016
J. Phys. Chem. A 2021, 125, 6715−6721

(33) Rijs, A. M.; Oomens, J. IR Spectroscopic Techniques to Study Isolated Biomolecules. *Top. Curr. Chem.* **2014**, *364*, 1−42.
(34) Oomens, J.; Sartakov, B. G.; Meijer, G.; Helden, G. V. Gas Phase Infrared Mulitiple Photon Dissociation Spectroscopy of Mass Selected Molecular Ions. *Int. J. Mass Spectrom.* **2006**, *254*, 1−19.
(35) Martens, J.; Berden, G.; Gebhardt, C. R.; Oomens, J. Infrared ion spectroscopy in a modified quadrupole ion trap mass spectrometer at the FELIX free electron laser laboratory. *Rev. Sci. Instrum.* **2016**, *87* (10), 103108.
(36) Yang, N.; Duong, C. H.; Kelleher, P. J.; Johnson, M. A.; McCoy, A. B. Isolation of site-specific anharmonicities of individual water molecules in the $I^-\cdot(H_2O)_2$ complex using tag-free, isotopomer selective IR-IR double resonance. *Chem. Phys. Lett.* **2017**, *690*, 159−171.
(37) Dickenson, G. D.; Niu, M. L.; Salumbides, E. J.; Komasa, J.; Eikema, K. S. E.; Pachucki, K.; Ubachs, W. Fundamental Vibration of Molecular Hydrogen. *Phys. Rev. Lett.* **2013**, *110* (19), 193601.
(38) Zhao, Y.; Truhlar, D. G. The M06 suite of density functionals for main group thermochemistry, thermochemical kinetics, noncovalent interactions, excited states, and transition elements: two new functionals and systematic testing of four M06-class functionals and 12 other functionals. *Theor. Chem. Acc.* **2008**, *120* (1), 215−241.
(39) Dolg, M.; Wedig, U.; Stoll, H.; Preuss, H. Energy-adjusted ab initio pseudopotentials for the first row transition elements. *J. Chem. Phys.* **1987**, *86* (2), 866−872.
(40) Dunning, T. H.; Hay, P. J. Gaussian Basis Sets for Molecular Calculations. In *Methods of Electronic Structure Theory*; Schaefer, H. F., Ed.; Springer US: Boston, MA, 1977; pp 1−27.
(41) Frisch, M. J.; Trucks, G. W.; Schlegel, H. B.; Scuseria, G. E.; Robb, M. A.; Cheeseman, J. R.; Scalmani, G.; Barone, V.; Mennucci, B.; Petersson, G. A.; et al. *Gaussian 09*, Revision D.01; Gaussian, Inc.: Wallingford, CT, 2009.
(42) Kamrath, M. Z.; Garand, E.; Jordan, P. A.; Leavitt, C. M.; Wolk, A. B.; Van Stipdonk, M. J.; Miller, S. J.; Johnson, M. A. Vibrational Characterization of Simple Peptides Using Cryogenic Infrared Photodissociation of $H_2$-Tagged, Mass-Selected Ions. *J. Am. Chem. Soc.* **2011**, *133* (16), 6440−6448.
(43) Marsh, B. M.; Zhou, J.; Garand, E. Vibrational spectroscopy of small hydrated $CuOH^+$ clusters. *J. Phys. Chem. A* **2014**, *118* (11), 2063−2071.
(44) Mitra, S.; Duong, C. H.; McCaslin, L. M.; Gerber, R. B.; Johnson, M. A. Isomer-Specific Cryogenic Ion Vibrational Spectroscopy of the $D_2$-Tagged $Cs^+(HNO_3)(H_2O)_{(n=0\text{-}2)}$ Complexes: Ion-Driven Enhancement of the Acidic H-Bond to Water. *Phys. Chem. Chem. Phys.* **2020**, *22* (8), 4501−4507.
(45) Kamrath, M. Z.; Relph, R. A.; Guasco, T. L.; Leavitt, C. M.; Johnson, M. A. Vibrational Predissociation Spectroscopy of the $H_2$-tagged Mono- and Dicarboxylate Anions of Dodecanedioic Acid. *Int. J. Mass Spectrom.* **2011**, *300*, 91−98.
(46) Johnson, C. J.; Wolk, A. B.; Fournier, J. A.; Sullivan, E. N.; Weddle, G. H.; Johnson, M. A. Communication: He-Tagged Vibrational Spectra of the $SarGlyH^+$ and $H^+(H_2O)_{2,3}$ Ions: Quantifying Tag Effects in Cryogenic Ion Vibrational Predissociation (CIVP) Spectroscopy. *J. Chem. Phys.* **2014**, *140* (22), 221101.
(47) Duong, C. H.; Yang, N.; Johnson, M. A.; DiRisio, R. J.; McCoy, A. B.; Yu, Q.; Bowman, J. M. Disentangling the Complex Vibrational Mechanics of the Protonated Water Trimer by Rational Control of Its Hydrogen Bonds. *J. Phys. Chem. A* **2019**, *123* (37), 7965−7972.
(48) Bendtsen, J. The rotational and rotation-vibrational Raman spectra of $^{14}N2$, $^{14}N^{15}N$ and $^{15}N2$. *J. Raman Spectrosc.* **1974**, *2* (2), 133−145.
(49) Wolk, A. B.; Leavitt, C. M.; Fournier, J. A.; Kamrath, M. Z.; Wijeratne, G. B.; Jackson, T. A.; Johnson, M. A. Isolation and characterization of a peroxo manganese (III) dioxygen reaction intermediate using cryogenic ion vibrational predissociation spectroscopy. *Int. J. Mass Spectrom.* **2013**, *354*, 33−38.


https://doi.org/10.1021/acs.jpca.1c05016
J. Phys. Chem. A 2021, 125, 6715−6721